Journal of
Flood Risk Management

A methodology for flood susceptibility and vulnerability analysis in complex flood scenarios

Francesco Dottori[1], Mario Lloyd Virgilio Martina[2] and Rui Figueiredo[2]

1 European Commission – Joint Research Centre, Institute for Environment and Sustainability, Ispra, Italy
2 IUSS – Institute for Advanced Studies, Pavia, Italy

Correspondence
Francesco Dottori, European Commission – Joint Research Centre Institute for Environment and Sustainability, Via E. Fermi 2749 Ispra Varese 21027 Italy
Tel: +390332789473
Email: francesco.dottori@jrc.ec.europa.eu

DOI: 10.1111/jfr3.12234

Key words
Flood damages; fluvial; risk assessment; vulnerability.

Abstract

Nowadays, flood risk management is gaining importance in order to mitigate and prevent flood disasters, and consequently the analysis of flood risk components is becoming a key research topic. In this paper, we propose a methodology for large-scale analysis of flood susceptibility and vulnerability. The methodology is based on a mathematical index, which considers local topography and basic information about the flood scenario to reproduce flooding processes. Its application allows for considering different levels of complexity of flood scenarios, from localized flood defence failures to complex hazard scenarios involving river reaches. The methodology synthesizes the spatial distribution of the index values into maps and curves that can be used to rank the susceptibility and implement a vulnerability analysis in the area of interest. The components of the methodology are tested in two flood plain areas in Northern Italy recently affected by floods. The results show that the methodology can provide an original and valuable insight of flood susceptibility and vulnerability processes.

Introduction

In recent years, strategies for the mitigation and prevention of flood disasters have shifted from a 'flood defence' approach, aimed at controlling the hazard by means of structural measures, to a 'flood management' approach, based on comprehensive risk assessment studies and costs and benefits analyses (Messner and Meyer, 2006; Merz *et al.*, 2010; Fuchs *et al.*, 2011). Following this trend, an increasing number of flood risk modelling tools are becoming available, ranging from simpler approaches to sophisticated methodologies involving hydrological and hydraulic models (Winsemius *et al.*, 2013). However, there are still unresolved issues in the application of flood risk models.

First, there is usually an imbalance in the relative importance given to the different components of risk. A key part of risk assessment studies consists in the estimation of the vulnerability of flood-prone areas, that is, the consequences that could be caused, in terms of damage and loss, by flood events of different magnitudes (Cutter *et al.*, 2013; Papaioannou *et al.*, 2015). However, while considerable efforts are often put into flood hazard evaluation, much less elaborated methods are usually applied for damage and loss assessment (Merz *et al.*, 2010). The exposure component of flood risk models can also be a source of considerable uncertainties (Figueiredo and Martina, 2016).

Second, consistent flood risk assessment requires taking into account all the possible sources of hazard in order to estimate the likelihood of a given area of being hit by a flood of a certain intensity, which is referred to, in the context of the present study, as flood susceptibility. However, in many cases, for instance in flood plain areas protected by multiple embankments, this would require the evaluation of a large number of flood scenarios, each one characterized by its magnitude and probability. Despite the continuing advances in flood hazard models, this type of probabilistic analysis is, in practice, not always feasible, due to a too large computational burden. As such, flood susceptibility analysis for complex scenarios is generally performed using Geographic Information System (GIS) approaches that take into account different layers of information, such as land use, elevation or existing flood maps (Manfreda *et al.*, 2011; Jalayer *et al.*, 2014; Tehrany *et al.*, 2014). Although simple and fast, the results cannot be compared with hydraulic models, as the level of information provided is often only qualitative (i.e. flood–no flood).

This calls for more balance between the different components of flood risk, adopting methods able to balance complexity (i.e. ease of application) and reliability (i.e. quantitative and consistent results).

Given this framework, in the present paper we propose a methodology designed for a lumped, large-scale evaluation of

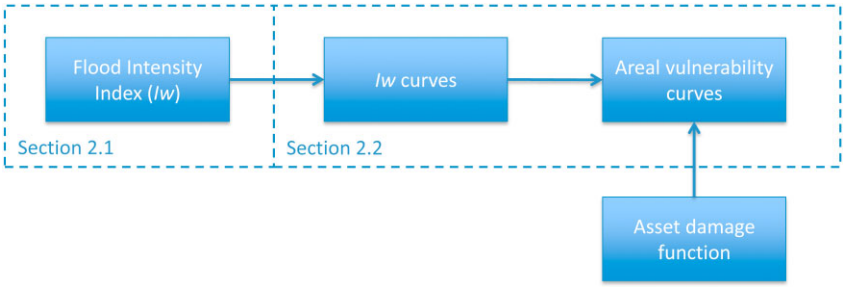

Figure 1 Conceptual scheme of the methodology.

flood susceptibility and vulnerability. The methodology is based on a GIS-based index called Flood Intensity Index (*Iw*), which can be considered as a trade-off between morphometric indexes and physically based two-dimensional (2D) hydraulic models. The index is designed to combine the ease of application of geomorphological indexes with a simplified, but physically sounding, description of flooding processes, considering the local topography, terrain roughness and basic information about the flood scenario.

The proposed methodology uses the aforementioned *Iw* index for providing an insight of flood variables and processes, considering both simple (e.g. local failure of flood defences) and complex hazard scenarios (e.g. failure or overflowing from one or multiple river reaches). According to the chosen strategy, the methodology synthesizes the information regarding the flood susceptibility of an area into graphs and curves. By combining this information with appropriate damage functions, the flood vulnerability of the area, relating the different flood scenarios with the damage they are expected to originate, can then be computed effortlessly. Additionally, the result of these analyses can be used to characterize, compare and rank the susceptibility and vulnerability of different flood-prone areas within a region (Tehrany *et al.*, 2014; Domeneghetti *et al.*, 2015).

The *Methodology* section provides a detailed description of the methodology and the rationale behind its development. The components of the methodology, especially the Flood Intensity Index, are tested in two flood plain areas in Northern Italy, as described in *Applications*. *Results and discussions* section presents the results of the application and discussions, while the last section presents the conclusions.

Methodology

The proposed methodology comprises two main parts, which are described in detail herein. First, in *The Flood Intensity Index* subsection, the theoretical background and the computing algorithm of the Flood Intensity Index are described. Second, in sub-section *Flood susceptibility and areal vulnerability analyses*, the possible applications of *Iw* results for the purpose of performing flood susceptibility and areal vulnerability assessments are presented and analysed, both for simple single-source flood scenarios and for complex ones with multiple possible sources. The methodology is conceptually represented in Figure 1.

The Flood Intensity Index

Dottori and Martina (2012) presented a preliminary version of the Flood Intensity Index (*Iw*), based on the existing GIS functions to compute non-Euclidean distances and paths. In the present work, we derive a generalized formulation based on an iterative method, which reproduces flow dynamics in case of slow and gradually varied flow.

The theoretical background stems from the 1D uniform flow equation written for large rectangular channels:

$$\frac{dH}{dx} = -\frac{V^2 n^2}{h^{4/3}} \tag{1}$$

where dH/dx is the water surface slope, V is the flow velocity, h is the water depth and n is the Manning coefficient. Eqn (1) can be discretized over regular grids and written as:

$$\frac{(H_i - H_j)}{d} = -\frac{V^2 n^2}{h^{4/3}} \tag{2}$$

where H_i and H_j are the water levels in two adjacent cells i and j, and d is the distance between these cells. In Eqn (2), the right-hand term can be seen as a single coefficient λ, embodying all the distributed head losses along d. Therefore, it is possible to use the equation to estimate the water level in the cell i:

$$H_i = H_j - \lambda \cdot d \tag{3}$$

If we indicate the cell j as the source of flow (i.e. with higher water level than cell i), we can define the Flood Intensity Index (Iw) for the cell i as:

$$Iw_i = H_{source} - Z_i - \lambda \cdot d \tag{4}$$

where Z_i is the elevation of the i-th cell.

Journal of Flood Risk Management published by The Chartered Institution of Water and Environmental Management and John Wiley & Sons Ltd

a (**11**)	b (**10**)	c (**9**)
d (**12**)	e (**11**)	f (**10**)
g (**13**)	h (**12**)	j (**11**)

Figure 2 Elevation grid for illustrating the computation of *Iw*.

For practical applications over 2D grids, *Iw* is computed through a two-step iterative scheme. For sake of simplicity, here we consider a case with a single-source cell.

At each iteration, Eqn (4) is first used to determine how many cells can be reached by water flow (i.e. *Iw* is > 0, step 1). The number of cells nc_{flow} is then used to modify Eqn (4) and compute the actual values of *Iw* for each *i*-th adjacent cell (step 2):

$$Iw_i = H_{source} - Z_i - \lambda \cdot d_{i,source} \cdot nc_{flow} \quad (5)$$

where H_{source} is the hydraulic head over the source cell and nc_{flow} is the number of cells identified in step 1 of the iteration. As can be seen, Eqn (5) computes higher losses in respect to Eqn (4) when flow can spread to multiple cells, thus partially accounting for flow lamination. Any cell for which a negative value is computed is assigned a 0 value.

In the present version of the algorithm, the head loss coefficient λ is computed as a weighted average of the slope along the flow direction and a reference value λ_r. λ_r is assigned based on the cell land use, similar to the Manning roughness coefficient. If the local slope is greater than λ_r, λ increases to simulate higher losses due to faster flow, while the opposite occurs for terrain slopes smaller than λ_r.

In each subsequent iteration, the algorithm locates the cell with the current maximum value of I*w,* which is taken as the new reference (or source) cell. Therefore, for the *i*-th adjacent cell we have:

$$Iw_i = (Iw)_{ref} + \left(Z_{ref} - Z_i - \lambda \cdot d_{i,ref} \cdot nc_{flow}\right) \quad (6)$$

where $(Iw)_{ref}$ is the index value for the reference cell. Note that the *i*-th cell might have already received an Iw value from previous iterations. In this case, the new value is assigned only if it is higher than the previous value (i.e. the new flow path has smaller head losses). The procedure is iterated until all cells with Iw > 0 have been considered as reference cells.

To illustrate how the computations are performed, let us assume a DEM of nine cells at 10 m resolution (Figure 2). Each cell is identified by a letter; the elevation of each cell is indicated between parentheses (in meters). Cell *h* is the source cell; therefore, its elevation is used as the reference water level. The λ coefficient is always set to 0.01, i.e. terrain slope is not considered for sake of simplicity. Therefore, head losses are equal to 0.1 m for flows in horizontal and vertical directions, and 0.14 m for diagonal flows.

-0.14	**0.9**	**1.86**
-1.10	**S**	**0.9**

0	**0.7**	**1.58**
0	**S**	**0.7**

Figure 3 *Iw* values computed after step 1 (left) and step 2 (right) of the first iteration.

	1.02	**2.18**
0	**0.7**	**1.58**
0	**S**	**0.7**

0	**1.2**	**2.18**
0	**0.7**	**1.58**
0	**S**	**0.7**

Figure 4 *Iw* values computed after the second iteration (left) and at the end of the iteration process (right).

Step 1 of the first iteration, performed using Eqn (4), results in the *Iw* values visible in Figure 3 (left). Since three cells receive a positive *Iw* value in this iteration, nc_{flow} is set equal to 3. The cells with negative values are not reached by flow and therefore are assigned a 0 value. Therefore, in step 2, *Iw* values are computed using Eqn (5), with the results shown in Figure 3 (right).

The second iteration takes as reference the cell with the highest value, which is (f). The final *Iw* values at the end of the second iteration show the propagation to cells (b) and (c), as shown in Figure 4 (left). Note that new *Iw* values are also computed for neighbour cells (e, j) with the previous index value. However, the new values are lower and therefore the previous values are retained.

For the third iteration, the reference cell would now be (c); however, the *Iw* values computed for adjacent cells (b, e, f) are all lower than previous values, and therefore are discarded. The same happens for the following iteration steps considering cells (b) and (j).

Instead, the *Iw* value computed using cell (e) is higher than previous value for cell (b), and therefore the value is updated. Finally, cell (a) is not reached by flow because the *Iw* value on adjacent cells (b), (e) is not high enough to generate a positive value.

Since all cells with positive *Iw* values have been considered, computations are stopped and the final grid of $\underline{Iw}$ values is shown in Figure 4.

Flood susceptibility and areal vulnerability analyses

Single-source flood scenarios

The most straightforward application of *Iw* is to consider a simple flood scenario with one localized hazard source. Possible examples are a localized dyke failure, or a section of a

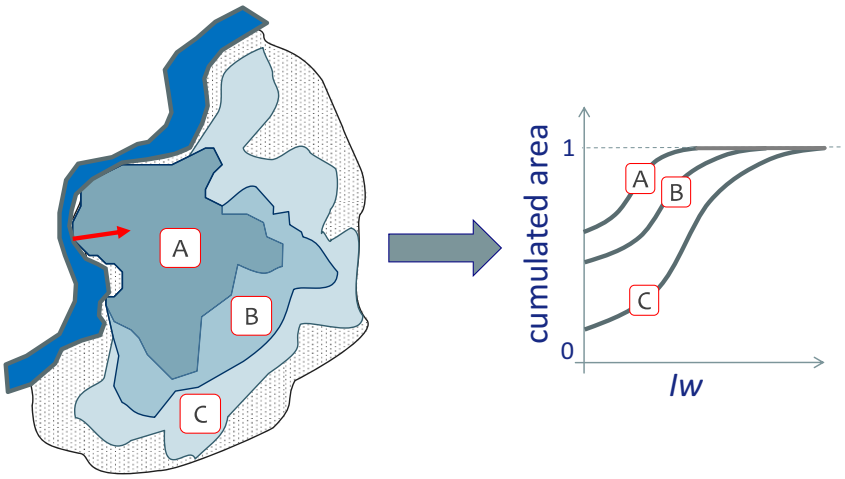

Figure 5 Conceptual scheme of the derivation of *Iw* curves. Note that the value of cumulated area in each scenario referred to total flood prone area (dotted area in the left-hand scheme).

riverbank being overtopped. In this case, a reference water depth can be used as boundary condition to compute the spatial distribution of *Iw* over the area of interest.

Such an application is similar to standard applications of flood inundation models, and in this case, the algorithm will provide a map of *Iw* values similar to a map of maximum water depths.

However, the application of *Iw* can be further expanded. Let us consider a flood-prone area, where the total area potentially affected by flooding can be clearly identified (e.g. a low land region bounded by levees and embankments). In this area, we consider different flood scenarios, originated by the same hazard source, but with a different hydraulic boundary condition, (e.g. varying water level in the river reach). As *Iw* computations are based on local terrain characteristics which do not vary, if the boundary water level is varied by a specific ΔH, all the *Iw* values will be shifted by the same ΔH (excluding those areas that were previously not given a value). Therefore, in this case the index represents the 'flood-order' of each point of the study area, regardless of the absolute value for flood. That is, the area can be 'classified' according to relative values of *Iw*, from the most to the least flood prone sectors.

Moreover, the relation between *Iw* values and flooded area can be expressed as a curve for each scenario and plotted in the same graph for different scenarios. Figure 5 shows a conceptual scheme for this approach, which is useful to provide, at a glance, a comparison of flood prone areas in each scenario.

In order to investigate the relationship between damage and hazard variables for the study area, it is possible to apply the *Iw* index as a measure of hazard. *Iw* values can be considered as a proxy of maximum water depths, as discussed in the *Results and discussion*, and combined with depth-damage curves to derive a spatial distribution of damage. If we characterize each scenario using the reference water level on the source point (H_{source}), then the values of aggregated total damage in each scenario can be represented in a hazard-damage graph and linked to form an areal vulnerability curve, which characterizes the study area (Figure 6).

The main idea behind the development of the methodology, however, is not its application to single-source flood scenarios, since a relatively similar procedure could be carried out using a 2D hydraulic model. The true potential of the *Iw* calculation algorithm lies with its applicability to complex flood scenarios extremely efficiently in terms of computational effort, which enables the possibility of performing areal vulnerability analyses over very large regions in short amounts of time, as further described in *Complex flood scenarios* subsection.

Complex flood scenarios

A different approach to the use of *Iw* consists of analysing the flood susceptibility and vulnerability of a study area potentially prone to different, complex hazard sources, for instance a flood plain protected by dykes and surrounded by one or more watercourses. In such a case, a flooding could potentially originate at any point of the flood defences, and for different hydraulic conditions in the rivers.

As previously mentioned, the application of standard 2D hydrodynamic models to combine all the possible hazard combinations would be complex and computationally demanding. On the contrary, the iterative algorithm of *Iw* can easily handle linear sources of hazard at the same time, since only the maximum values of *Iw* are used in the computation. Using the algorithm in such a way allows for an effortless quantification of the maximum flood intensity

Journal of Flood Risk Management published by The Chartered Institution of Water and Environmental Management and John Wiley & Sons Ltd

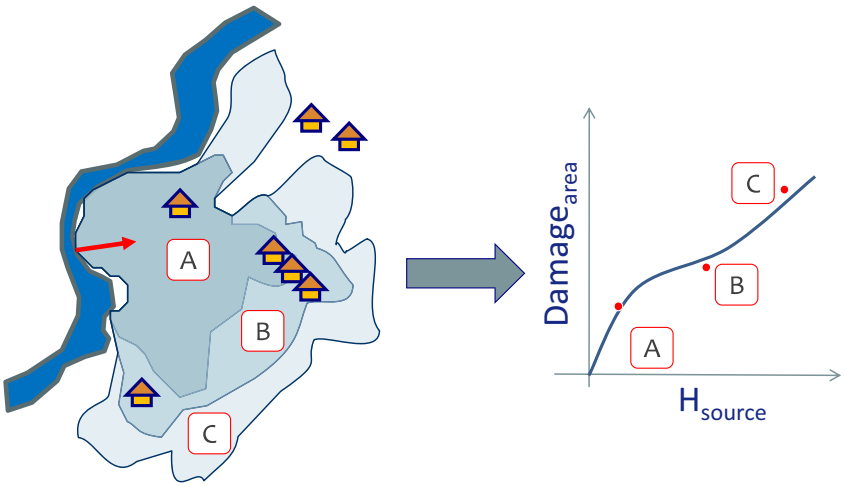

Figure 6 Conceptual scheme of the derivation of areal vulnerability curves.

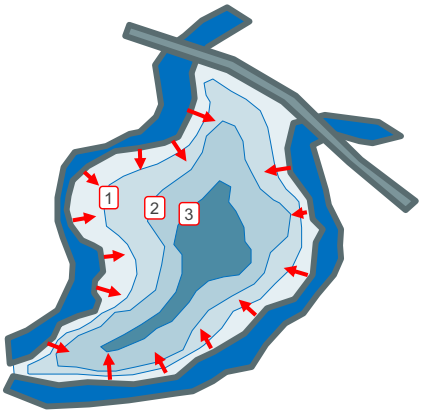

Figure 7 Conceptual scheme of the application of the *Iw* index to complex flood scenarios.

indexes in the study area. Boundary condition can be given by water levels in the reaches of interest, for instance coming from in-site measurements or 1D modelling of flood scenarios. Different scenarios can be analysed, for instance considering the water levels related to a specific flood return period. In case of an area bounded by more than one water course, each scenario can consider a different combination of boundary conditions in the rivers concerned (Figure 7). With respect of the strategy described in *Single-source flood scenarios* subsection, this application is not related to a specific flood scenario, but can instead provide an indication of the spatial distribution of maximum *Iw* in the study area given a large number of potential hazard sources.

Alternatively, a Monte-Carlo simulation based approach can be carried out, where instead of considering a linear hazard source, a large number of single sources along the river reach are used. This approach allows not only the quantification of the maximum flood intensity indexes in the area (which are the maximum *Iw* values for each cell from all the runs), but also to relate the index with its probability of occurrence, considering the number of sources that can originate it in relation to all the potential sources along the river reach. This enables the effective quantification of the flood susceptibility of the area and the generation of the respective susceptibility curves and maps. Additionally, depth-damage curves can be applied in order to perform an areal vulnerability and risk assessment.

Applications

The proposed methodology has been tested and applied in two test areas, located in the lowland part of the Emilia-Romagna Region, Northern Italy. Both sites have been affected by severe flood events in recent years caused by dyke failures. The location of test sites is shown in Figure 8.

Test areas

Area 1

The first test area is located at approximately 30 km north-east of the city of Bologna, next to the river Reno (Figure 8). The site is mainly used for agriculture, with sparsely distributed farm buildings and the small village of Malalbergo. The area of interest is entirely bounded by road embankments and dykes, and crossed by a motorway embankment. A drainage network composed by field tile drains and a main drain is also located in the site, as shown in Figure 9. The total extent is approximately 8 km^2.

A breach on the right levee of the Reno River caused the flooding of the test site in November 1990. The spill lasted about 10 h, with the maximum discharge peak estimated to be 200 m^3/s; the total flooded area was 5.6 km^2.

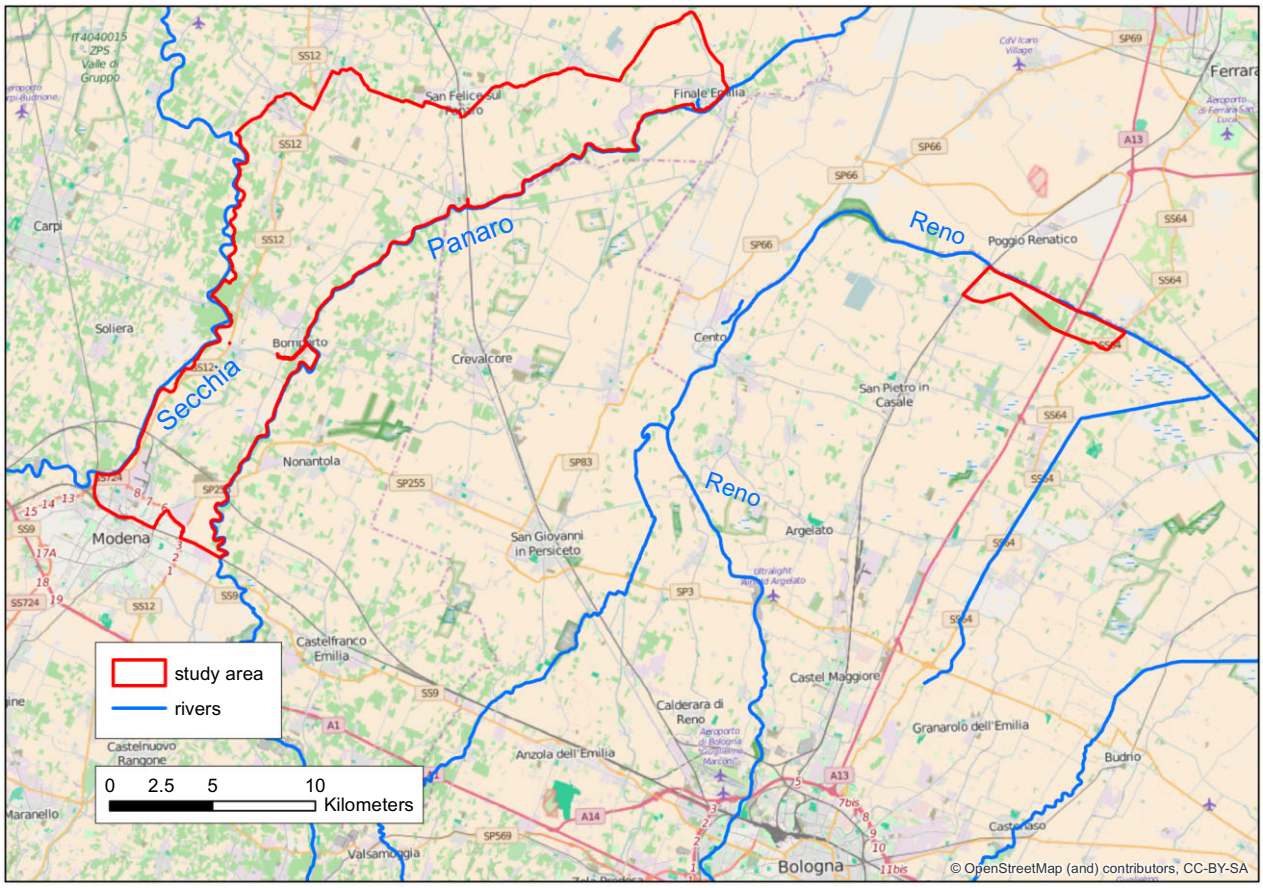

Figure 8 Location of the two study areas and main rivers of the area.

The 1990 flood event has been studied in previous research works (Dottori, 2012; Hailemariam *et al.*, 2014). These authors collected a comprehensive set of topographic data (including embankments and drainage network) and observations of flood extent and depth, which were used for the application and evaluation of the 2D hydrodynamic model CA2D.

Therefore, this case is used to test whether the flood intensity index values can be considered as a reliable proxy of water depths, by comparing *Iw* values against both observations and results from the CA2D model. In addition, the susceptibility and vulnerability of the area are evaluated through the curves described in *Single-source flood scenarios* subsection.

Area 2

The second test site has a total extent of around 200 km^2 and is located northeast of the city of Modena (Figure 8). It is a lowland agricultural area with several small towns, villages and sparsely distributed farm buildings. The site is bounded by the Secchia River on the NW side and by the Panaro River on the SE side, while the other boundaries are given by road embankments (Figure 10). As in Area 1, a complex drainage network is present in the site.

The test site was affected by flooding on January 2014 due to a dyke breach along the River Secchia. According to reconstruction of the event in the aftermath, the outflow continued for almost 48 h before repair works were able to close the breach, with a maximum discharge peak estimated to be 400 m^3/s. The total flooded area was ~ 90 km^2, including large sections of urban areas.

For this event, topographic information and flood footprints at different time steps have been collected; however, the level of detail is not as high as for area 1, since embankments and the drainage network could not be integrated in spite of their influence on flooding processes. Therefore, the case is used as a conceptual exercise for producing maximum vulnerability maps, as well as a benchmark for testing *Iw* performance in large areas.

Sensitivity analysis

The performance of the Flood Intensity Index in test area 1 is evaluated through a sensitivity analysis of the parameter

Journal of Flood Risk Management published by The Chartered Institution of Water and Environmental Management and John Wiley & Sons Ltd

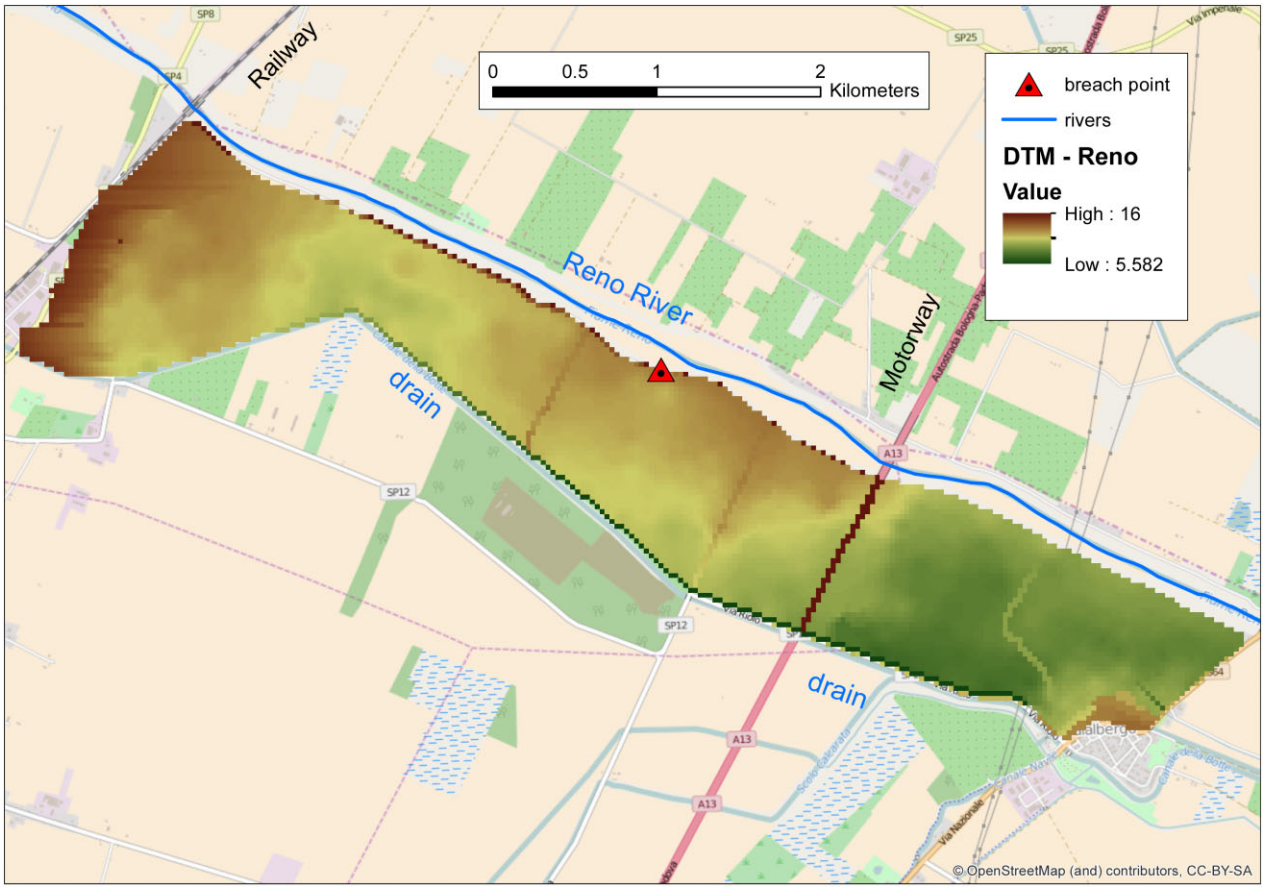

Figure 9 Detail of test area 1, with the location of the Reno River, the drain and the motorway and railway embankments.

space, following the usual approach applied for flood hazard models (Dottori, 2012).

For the present application, we focus the analysis on the loss coefficient λ, using two different values for the drainage network and for the flood plain areas. The reference water level over the source point H_{source} has been set equal to the average water depth (0.7 m) computed from the reconstructed breach hydrograph (Hailemariam *et al.*, 2014).

The flood extent computed through *Iw* is compared against observed maximum flood extent using the performance indexes P1, P2 proposed in Hunter *et al.* (2005):

$$P1 = W1/(W1 + W0 + D0)$$
$$P2 = (W1 - W0)/(W1 + W0 + D0) \quad (7)$$

where W1 is the area that is correctly predicted as flooded in the model, W0 is the area wrongly predicted as flooded in the model, D0 is the flooded area not predicted by the model simulation.

Iw values in correspondence of high water marks are evaluated using absolute and relative root mean square error (RMSE). The performances in terms of P1, P2 and RMSE are also compared with the results of the CA2D model described in Dottori (2012).

Derivation of areal susceptibility and vulnerability curves

In order to derive areal susceptibility and vulnerability curves for test site 1, the flood event of 1990 has been considered together with two additional, higher magnitude flood scenarios. The latter (S2 and S3) are derived considering the same breach location, while reference water depth used for simulating the 1990 event has been increased by 50% and 100%, respectively. The 1990 scenario is indicated as S1.

Based on the results obtained in the sensitivity analysis (described in *Sensitivity analysis* subsection), the values of the coefficient λ have been set to 0.0002 for the drainage network, and 0.0003 for the flood plain area.

To compute the areal vulnerability curves, we adopted the depth-damage functions developed by Huizinga (2007). The functions are derived from a database of existing studies for several European Countries, and classify asset values into five

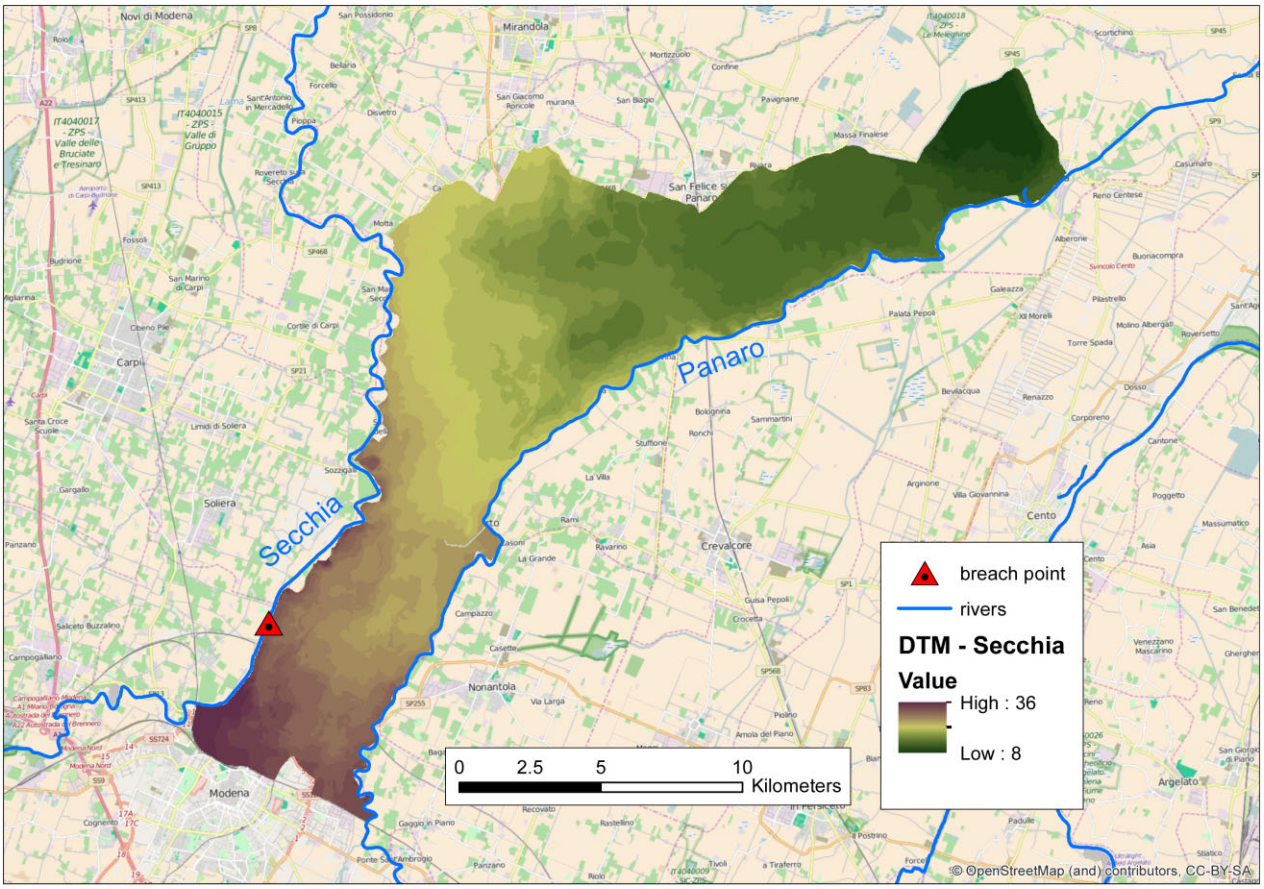

Figure 10 Detail of test area 2, with the location of Secchia and Panaro rivers.

damage classes: residential, commercial, industrial, roads and agriculture. Exposure is derived from the Corine Land Cover map and is scaled to the GDP per capita. Although the damage model has been successfully tested in two case studies in Germany and England (Jongman *et al.*, 2012), its reliability for Italy has not yet been tested. Therefore, the present application should be regarded as a conceptual exercise, as a detailed validation would be beyond the scope of this paper. The curves derived for the test case are described in *Susceptibility and areal vulnerability graphs*.

Derivation of maximum Flood Intensity Index maps

To analyse the flood susceptibility of the study area 2, the *Iw* index has been computed considering the two embankments bounding the area (Figure 6) as linear, continuous hazard sources (that is, every grid cell on these borders is considered as a source cell). The dike breach occurred in 2014 has been taken as reference to define the magnitude of the flood scenarios: in each source cell, the reference water level has been defined as the local bottom elevation of the embankment, plus the average water depth computed from the reconstructed breach hydrograph (1.2 m). Given the comparable discharge of the rivers Secchia and Panaro, the same reference depth has been used. In practice, such a schematization implies a uniform failure probability of the defence structures, since no information on geometrical and geotechnical conditions of the embankments is available. The curves derived for the test case are described in *Maximum Flood Intensity Index maps*.

Results and discussions

Sensitivity analysis

The performance of *Iw* in reproducing the observed flood extent is presented in Figure 11, showing the scores of the indexes P1 and P2 as a function of flood plain and drain loss coefficients (λ). The comparison between watermarks and local *Iw* values considering absolute and normalized RMSE is shown in Figure 12.

Journal of Flood Risk Management published by The Chartered Institution of Water and Environmental Management and John Wiley & Sons Ltd

As can be seen from the graphs, it is not possible to find a calibration that maximizes the index performance against both the observed data types. The increase of the loss coefficient λ improves index performance against point measurements, whereas flood extent is better reproduced by decreasing λ. Relatively, good results are obtained for λ values of $3{\cdot}10^{-4}$ and $2{\cdot}10^{-4}$, respectively, for the flood plain and the drain: with this set of values, the P2 index produces a 0.75 value, while RMSE in respect to observed depths is 51 cm. Although such errors are not negligible, they are relatively close to the results of CA2D model obtained by Dottori (2012). Using the optimum calibration for the model parameters, the author reported an RMSE on observed depths of 32 cm, and a value of P2 index of 0.84. Figures 13 and 14 show a visual comparison of results for CA2D and *Iw* in terms of flood extent. In addition, the same author observed some incoherencies between high water marks and observed flood extent, meaning that observed data sets are also affected by errors.

The *Iw* performance could probably be improved by setting a localized higher value of λ for the motorway underpass, to reproduce concentrated head losses due to the narrowing of flow section; however, this has not been done to avoid over-parameterization.

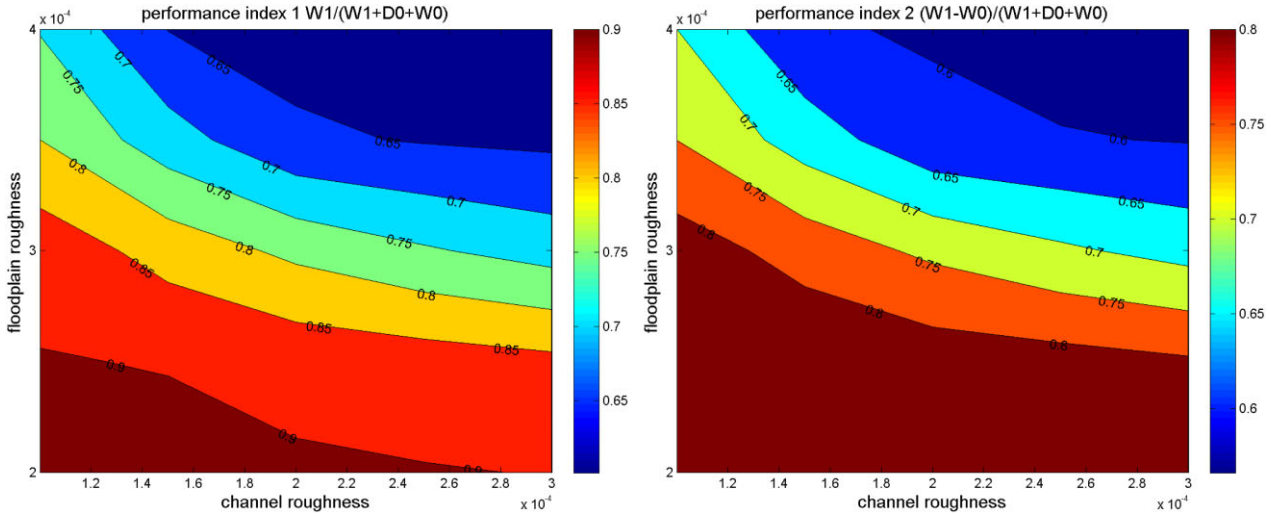

Figure 11 Values of the performance indexes P1 (left) and P2 (right) as a function of flood plain and drain loss coefficients (λ).

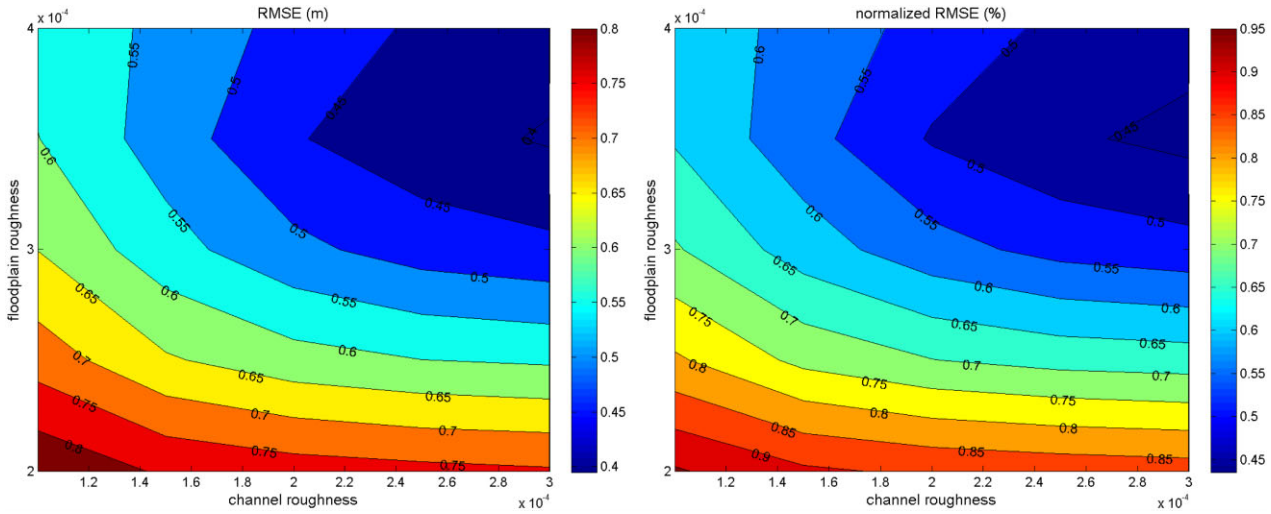

Figure 12 Variation of root mean square error (RMSE) (left) and normalized RMSE (right) between *Iw* values and observed water marks as a function of flood plain and drain loss coefficients (λ).

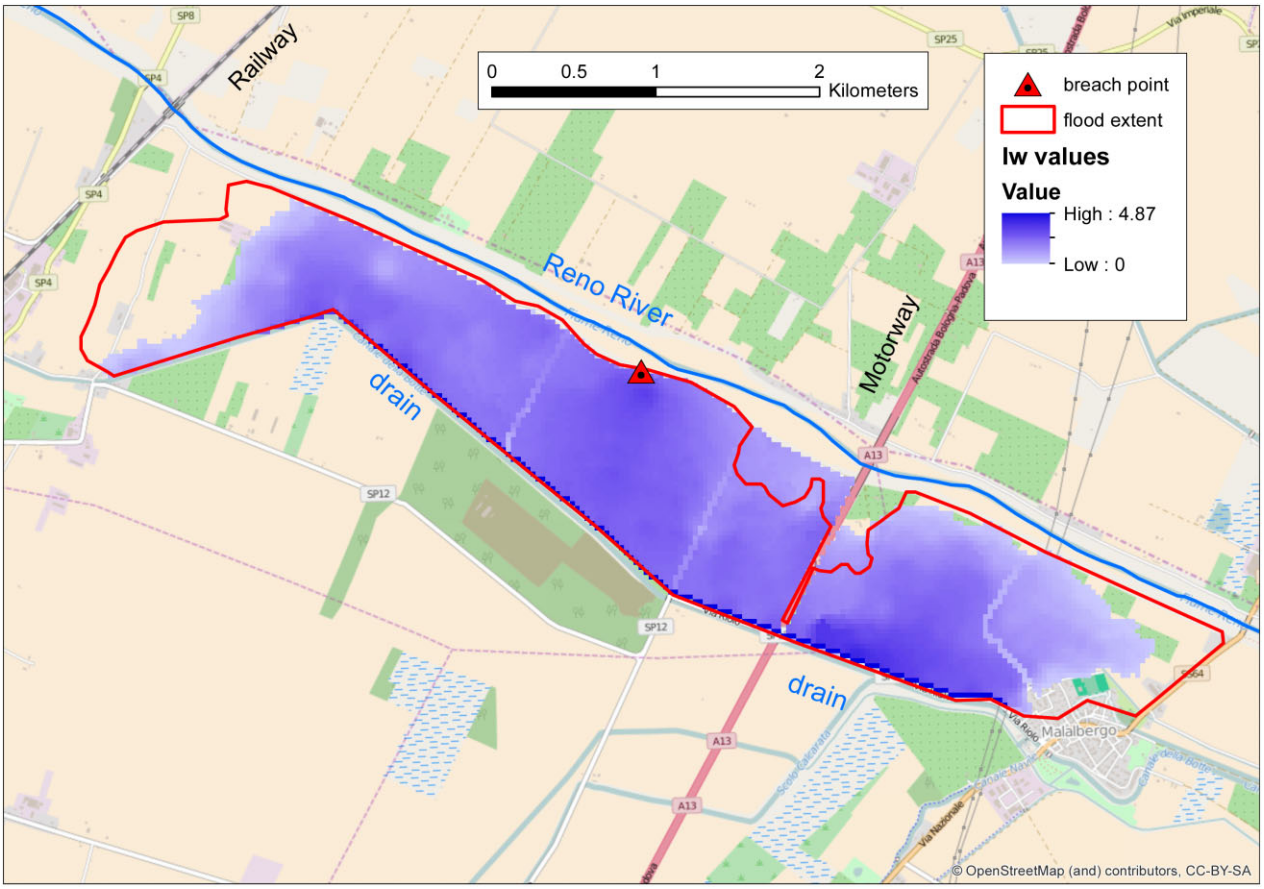

Figure 13 Map of *Iw* values (λ values: 0.0003 for flood plain and 0.0002 for drain), compared with the observed flood extent.

Susceptibility and areal vulnerability graphs

Figure 15 shows the *Iw* curves (*Iw* values against cumulated area) for the three flood scenarios considered. S1 corresponds to the 1990 flood event, while S2 and S3 are obtained considering a source water depth increased by 50% and 100%, respectively.

As can be seen, the areal curves can be used to characterize at a glance the flood susceptibility in each scenario, allowing for quick comparisons. For instance, only a limited fraction of the area is not reached by water (more than 20% for S1, 10% for S3). Also, the highest values of *Iw* (more than 1.5 m for S1, more than 2.2 m for S3) involve a very small fraction of the total area, corresponding to cells close to the drainage channel.

Figure 16 reports the areal vulnerability curves (reference water depth H_{ref} on the breach point versus total damage) for the three flood scenarios.

It is interesting to note how the damage shows a marked increase from scenario S1 to S2, despite a limited increase in flood extent (from 5.31 to 6.28 km^2). This is due to the fact that in scenario 1 most of the village of Malalbergo is not reached by flooding, while it happens for scenario 2.

Maximum Flood Intensity Index maps

The map of *Iw* values obtained considering multiple linear sources has been normalized and classified, and is shown in Figure 17. Before commenting the results, it is important to note that the *Iw* values computed are affected by the partial representation of local topography; as mentioned in *Applications*, the Digital Terrain Model (DTM) DTM used does not include road and river embankments or the drainage network, which in a real situation would largely alter flow paths. Moreover, the use of DTM to determine the local bottom elevation of embankments for source cells means that probably some cells were given a higher elevation, thus giving additional 'head' to *Iw* computations. Therefore, the results here shown should be analysed from a conceptual point of view, and not used to draw conclusions about the real susceptibility conditions in the area.

A number of interesting considerations can be drawn from the results. First, the map of Figure 17 shows that in this area, *Iw* values are mainly driven by elevation rather than distance from embankments, which is an expected result as all the points are relatively close to at least one embankment (max distance is ~ 7 km).

Journal of Flood Risk Management published by The Chartered Institution of Water and Environmental Management and John Wiley & Sons Ltd

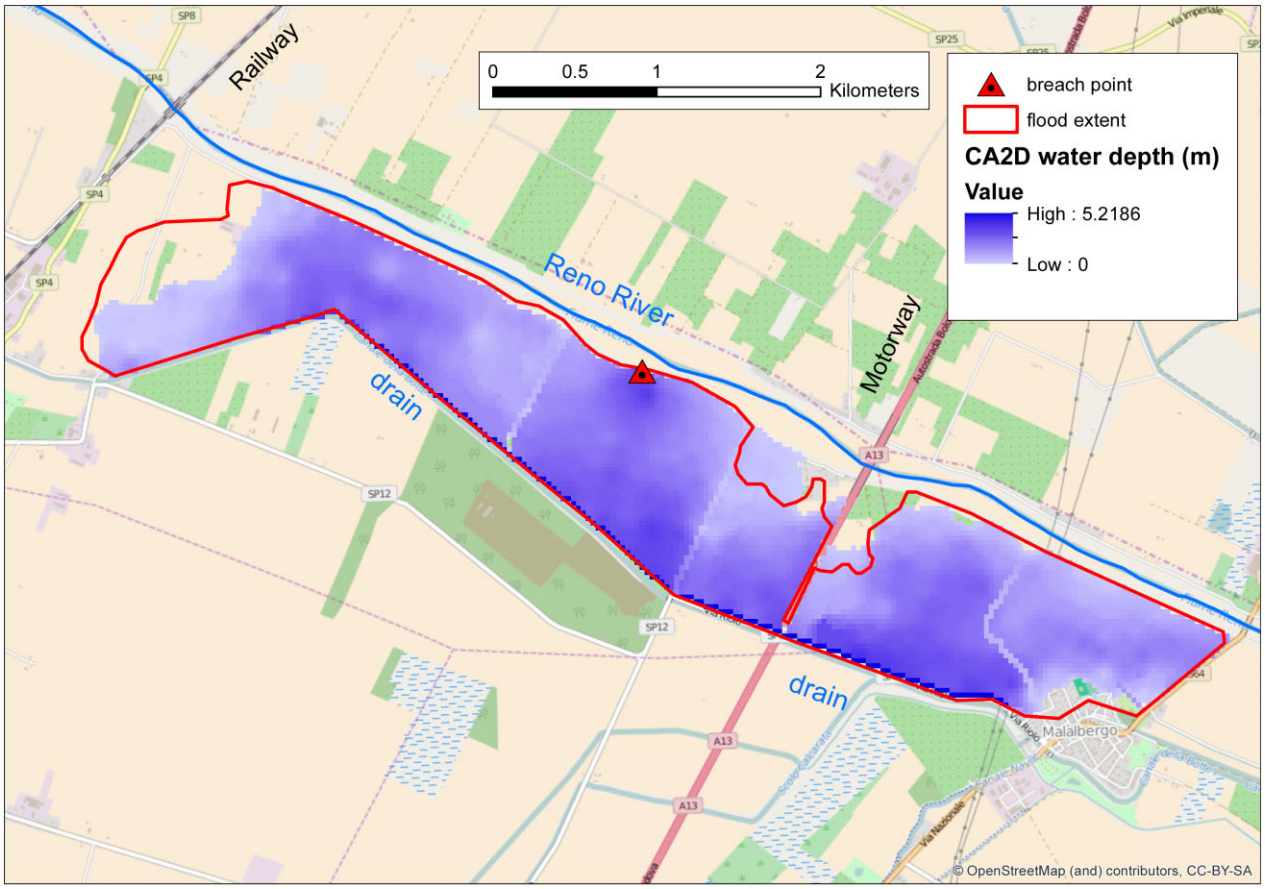

Figure 14 Map of CA2D maximum water depths (roughness values: 0.18 $m^{1/3}s$ for flood plain and 0.03 $m^{1/3}s$ for drain), compared with the observed flood extent.

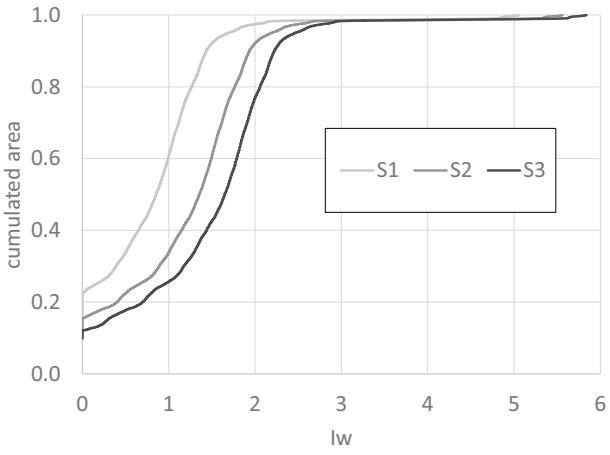

Figure 15 *Iw* curves for test area 1 for the three scenarios.

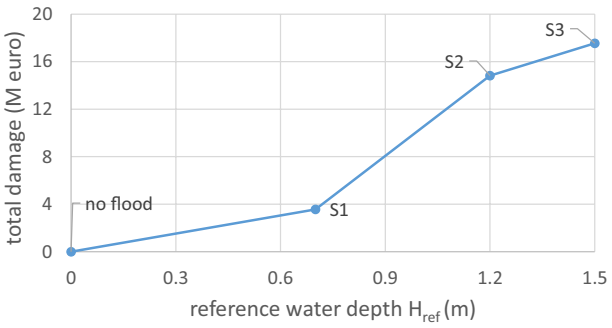

Figure 16 Areal vulnerability curves for test area 1 for the three scenarios.

However, the map does provide additional information that cannot be extracted by the DTM only. As can be seen, the areas with higher *Iw* values are those located in local depressions, while the cells located next to embankments have lower values due to their higher elevation. In particular, *Iw* distribution seems to be sensitive to local elevation difference rather than absolute elevation; in other words, *Iw* correctly classifies cells in local depressions as 'equally susceptible'.

This means that the map can also be interpreted as a probabilistic flooding map in which a uniform failure probability is assumed. Points at higher elevations might be flooded only if a dyke failure occurs nearby, while low-lying points, especially in local depressions, are more likely to be

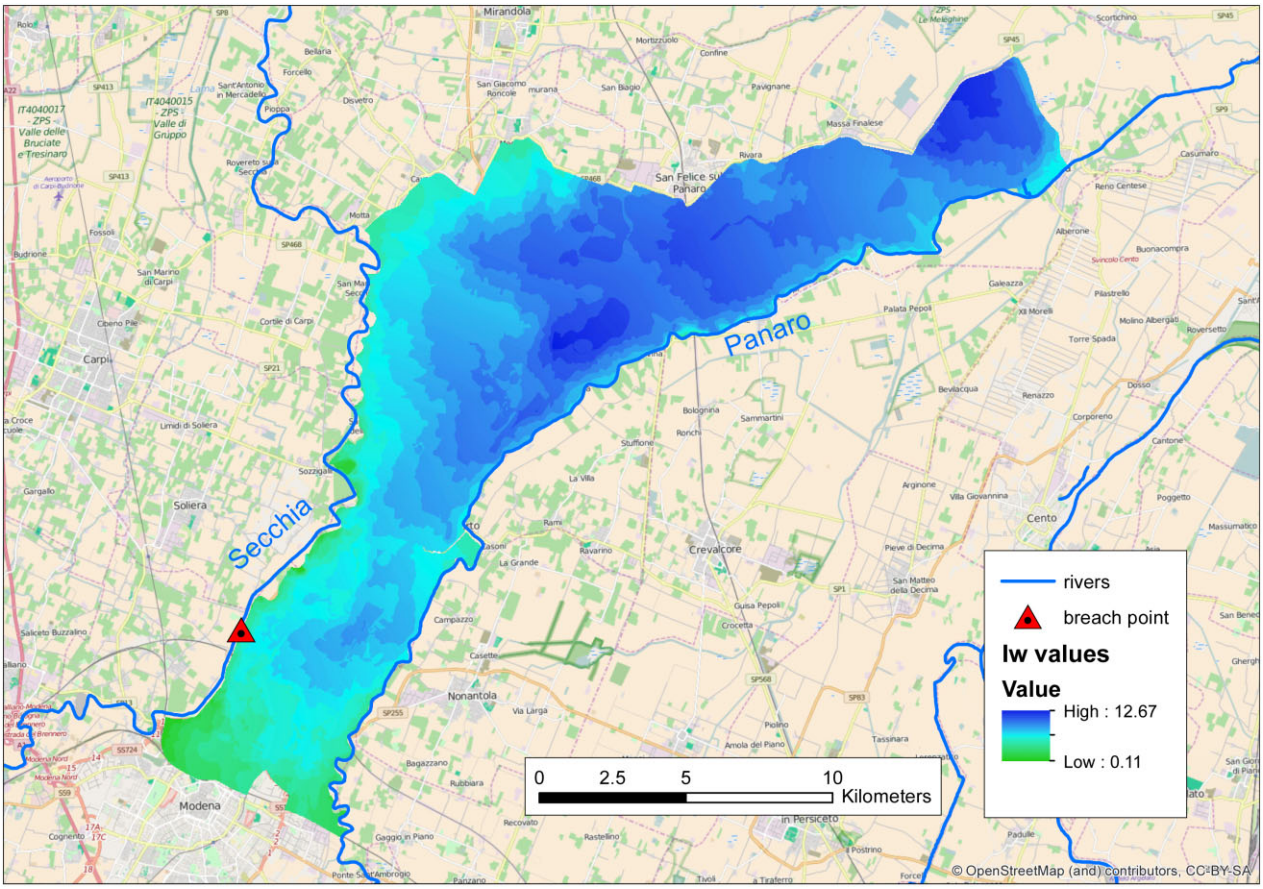

Figure 17 Map of relative values of *Iw* computed using multiple linear sources along the rivers Secchia and Panaro.

flooded regardless of the breach location. However, it is important to note that a real flood frequency analysis would require simulating a large number of flood scenarios with the related failure probability. Besides, it is important to mention again that *Iw* values are not taking into account important hazard variables: points located close to the rivers are less likely to be flooded, but if they were, higher velocities and more rapid inundation would probably cause more damage.

Additional discussions

Further considerations can be drawn on the applicability range of the Flood Intensity Index *Iw*. Since *Iw* is developed to provide a simplified representation of flooding processes, it is important to keep in mind the shortcomings applied to derive governing equations (see *The Flood Intensity Index* subsection). First, temporal evolution of flooding processes is not accounted for, as in practice, the algorithm represents a flooding process under steady flow conditions. This implies that flow velocity is not estimated. In addition, the current formulation of the loss coefficient λ is mainly a function of local land use, while there is only an indirect dependence on flow conditions, based on empirical relationships (higher losses are supposed on steeper slopes and where multiple flow directions). Better performances could be obtained through a further elaboration of the *Iw* formulation. For instance, a two-step procedure could provide a better estimation of flow depth term *h* within λ. In addition, a possible formulation to estimate velocity could be developed.

Besides limitations, a key strength of *Iw* is the use of water level as a measure of hazard. Water level in rivers can easily be related with discharge and magnitude of flow (i.e. return period), and can be estimated both by on-site measurements and simulations of 1D hydraulic models. Even if estimations of river water level are not available, a reference value can be set based on local ground (or embankment) elevation as shown in *Maximum Flood Intensity Index maps* section, provided that a physically sounding value of water depth is chosen.

Conclusions

The results of the applications described in this manuscript highlight the potential of the proposed methodology in providing quick, useful information for flood susceptibility and, eventually, vulnerability assessment.

Journal of Flood Risk Management published by The Chartered Institution of Water and Environmental Management and John Wiley & Sons Ltd

First, although extensive testing in further cases is needed, the first results are very promising and show that the Flood Intensity Index *Iw* can be a flexible and effective tool for analysing and mapping flooding processes. As expected, the results showed limitations due to the approximations applied (absence of temporal evolution of flow, no draining processes, no estimation of velocity), and it should be clearly understood that the analysis performed with *Iw* cannot reach the level of detail and accuracy of 2D hydraulic models. Nevertheless, the results show that the algorithm is able to represent reasonably well flow dynamics in low land areas.

Second, the reduced run times and the flexibility of the algorithm computing *Iw* are key aspects that allow for the application of new strategies for integrating complex, multisource flood scenarios into susceptibility and vulnerability analyses.

Maps of the spatial distribution of maximum Flood Intensity Index values in a given area of interest can be a useful resource for flood risk management and planning purposes. *Iw* maps can also be used in combination with appropriately defined stage-damage functions to derive areal vulnerability curves for a given area of interest.

Vulnerability and susceptibility curves and maps derived from a probabilistic calculation of complex scenarios can easily be compared among different regions, which enable the development of large-scale areal susceptibility analyses (e.g. country level).

Valuable information can also be obtained through the frequency analysis of flood hazard in a Monte-Carlo framework. The latter approach has not been tested in the present paper, as we felt that the reliability and potential of the proposed methodology could be better demonstrated in simple test cases, but it will be a key issue in forthcoming research work.

In other words, the proposed methodology shows that it is possible to 'compress' (i.e. synthesize) the information in a clever way, providing valuable information for susceptibility and vulnerability assessment at large scale, with a reduction of the resources used. Thus, it is possible to put the focus on other aspects, such as the analysis of a larger number of flood scenarios, or a more in-depth uncertainty analysis. Finally, it is important to point out that the proposed methodologies should not be seen in contrast with existing approaches for vulnerability assessment. The analyses and concepts here presented should be regarded as a preliminary, large-scale analysis to locate most vulnerable areas within a region, where more detailed analyses can then be performed.

Acknowledgements

The authors acknowledge the financial support for the publication of this paper by the European Commission, Joint Research Centre. The authors would like to thank Luc Feyen (European Commission, Joint Research Centre) for providing the functions and the computer code for flood damage estimation. Comments from two anonymous reviewers are also gratefully acknowledged.

References

Cutter S.L., Emrich C.T., Morath D.P. & Dunning C.M. Integrating social vulnerability into federal flood risk management planning. *J Flood Risk Manag* 2013, **6**, (4), 332–344.

Domeneghetti A., Carisi F., Castellarin A. & Brath A. Evolution of flood risk over large areas: quantitative assessment for the Po River. *J Hydrol* 2015, **527**, 809–823.

Dottori F. Development of parallelizable flood inundation models for large scale analysis. PhD Dissertation, University of Bologna, Italy, 2012.

Dottori F. & Martina M.L.V. Un metodo semplificato per la stima della vulnerabilità alluvionale. Atti del XXXIII Convegno Nazionale di Idraulica e Costruzioni Idrauliche, Brescia, Italy (in Italian), 2012.

Figueiredo R. & Martina M. Using open building data in the development of exposure datasets for catastrophe risk modelling. Accepted for publication in Natural Hazards and Earth System Sciences, 2016.

Fuchs S., Kuhlicke C. & Meyer V. Editorial for the special issue: vulnerability to natural hazards – the challenge of integration. *Nat Hazards* 2011, **58**, (2), 609–619.

Hailemariam F.M., Dottori F. & Brandimarte L. Investigating the influence of minor hydraulic structures on modelling flood events in lowland areas. *Hydrol Process* 2014, **28**, (4), 1742–1755. doi: 10.1002/hyp.9717.

Huizinga H.J. Flood damage functions for EU member states, HKV Consultants, Implemented in the framework of the contract #382442-F1SC awarded by the European Commission – Joint Research Centre, 2007.

Hunter N.M., Bates P.D., Horritt M.S., De Roo A.P.J. & Werner M.G.F. Utility of different data types for calibrating flood inundation models within a GLUE framework. *Hydrol Earth Syst Sci* 2005, **9**, (4), 412–430.

Jalayer F., De Risi R., De Paola F., Giugni M., Manfredi G., Gasparini P. & Renner F. Probabilistic GIS-based method for delineation of urban flooding risk hotspots. *Nat Hazards* 2014, **73**, (2), 975–1001.

Jongman B., Kreibich H., Apel H., Barredo J.I., Bates P.D., Feyen L., Gericke A., Neal J., Aerts J.C.J.H. & Ward P.J. Comparative flood damage model assessment: towards a European approach. *Nat Hazards Earth Syst Sci* 2012, **12**, 3733–3752.

Manfreda S., Di Leo M. & Sole A. Detection of flood prone areas using digital elevation models. *J Hydrol Eng* 2011, **16**, (10), 781–790.

Merz B., Kreibich H., Schwarze R. & Thieken A. Assessment of flood economic damage. *Nat Hazards Earth Syst Sci* 2010, **10**, 1697–1724.

Messner F. & Meyer V. Flood damage, vulnerability and risk perception – challenges for flood damage research. *Flood Risk Manag: Hazards, Vulnerability and Mitigation Measures* 2006, **67**, 149–167.

Papaioannou G., Vasiliades L. & Loukas A. Multi-criteria analysis framework for potential flood prone areas mapping. *Water Resour Manage* 2015, **29**, (2), 399–418.

Tehrany M.S., Pradhan B. & Jebur M.N. Flood susceptibility mapping using a novel ensemble weights-of-evidence and support vector machine models in GIS. *J Hydrol* 2014, **512**, 332–343.

Winsemius H.C., Van Beek L.P.H., Jongman B., Ward P.J. & Bouwman A. A framework for global river flood risk assessment. *Hydrol Earth System Sci* 2013, **17**, (5), 1871–1892.

Journal of Flood Risk Management published by The Chartered Institution of Water and Environmental Management and John Wiley & Sons Ltd